International Journal of Control, Automation and Systems 14(4) (2016) 1082-1095
http://dx.doi.org/10.1007/s12555-014-0568-4
ISSN:1598-6446 eISSN:2005-4092
http://www.springer.com/12555

Attitude Control for Astronaut Assisted Robot in the Space Station

Jinguo Liu*, Qing Gao, Zhiwei Liu, and Yangmin Li*

Abstract: Because of the limited working hours of astronauts in the space station, the in-cabin robot has high value in the technological validation and scientific research. Based on this requirement, we proposed and designed an Astronaut Assisted Robot(AAR) working in the space station. It can float in the space station cabin, fly autonomously, and hold a fixed position and/or posture. In addition, it also possesses environmental awareness capabilities and intelligence. Thus the AAR can assist astronauts to complete some special scientific experiments or technical tests. In this paper, the system architecture and experimental equipment of the AAR are designed firstly depending on the characteristics of space microgravity environment and the requirements of assisting astronauts missions. And then, the motion principles of the AAR are analyzed and the robot's dynamic model is established by using the Newton - Euler algorithm. Since the attitude control of the robot is the basis for its free movement, the PID Neural Network(PIDNN) algorithm, which is a kind of intelligent control algorithm, is used to design the attitude controller of the AAR. Finally, the reasonability of the robot's structural design and the availability of its attitude controllers are verified through the simulation experiments.

Keywords: Astronaut assisted robot, attitude control, PID Neural Network, space station.

1. INTRODUCTION

Around 2020, China will build up the near-earth Chinese Space Station which will be used to develop and test a number of advanced and core technologies and instruments in the field of space technology, which will provide solid support for the future development of China's manned deep space explorations [1–3]. Considering that there are serious problems from ISS's operational lessons that the available astronaut time is usually limited, it is necessary to design an in-cabin robot to assist the astronaut in the Chinese Space Station. As technical verification equipment or scientific application payload, this kind of robot can be used to assist astronauts to conduct some inter-vehicular activities [4]. Compared to ordinary scientific experimental satellites and unpressured space manipulators, the in-cabin robots must work in the space station cabin. The cabin can provide a better scientific experimental environment and a higher level of controllable environment.

The space station in-cabin robot has technical demonstration mainly includes: (a) Verifying six-degree-of-freedom control experiments including attitude control, minisatellites formation, and docking technology [5]. (b) Promoting the development of space robotics [6]. Meanwhile its scientific application mainly includes: (a) Monitoring in-cabin equipment, health management and assisting astronauts to work. (b) Isolating vibration effectively to carry scientific experimental loads. Compared to the traditional isolation platform currently used in ISS [7], the cabin floating platform does not need complex technology to create a high-level microgravity environment, and the experimental device is convenient and flexible.

During the ISS's building up and operation, there are some typical related projects in the world. One of them is the Synchronized Position Hold, Engage, Reorient, Experimental Satellites (SPHERES) project conducted by MIT. SPHERES is used to realize the experiments of six-degree-of-freedom control algorithms and these control algorithms include attitude control, minisatellites formation control and ministatellites docking control algorithm. In addition, they also try to make use of computer vision to position the SPHERES and machine intelligence is added to a certain extent to make the SPHERES become autonomous robots so that it behaves self-perception and self-movement [5, 9, 10]. Also, a cabin floating robot is

Manuscript received December 25, 2014; revised April 9, 2015 and June 20, 2015; accepted August 16, 2015. Recommended by Associate Editor Wen-Hua Chen under the direction of Editor Duk-Sun Shim. This work was supported in part by the National Science Foundation of China (51175494, 51575544), Macau Science and Technology Development Fund (108/2012/A3), the State Key Laboratory of Robotics Foundation, and Research Committee of University of Macau (MYRG2015-00194-FST).

Jinguo Liu, Qing Gao, and Zhiwei Liu are with the State Key Laboratory of Robotics, Shenyang Institute of Automation, Chinese Academy of Sciences, Shenyang 110016, China (e-mails: liujinguo@sia.cn, gaoqing@sia.cn, iamliuzhiweixyz@163.com). Qing Gao is also with University of the Chinese Academy of Sciences, Beijing 100049, China. Yangmin Li is with the Department of Electromechanical Engineering, University of Macau, Taipa, E11-4067, Macao SAR (e-mail: ymli@umac.mo).
* Corresponding authors.

named Personal Satellite Assistant(PSA) developed by NASA's AMS Research Center. PSA's main task is to help astronauts to work, as well as to undertake health management such as monitoring the air content, temperature and humidity of the ISS [8]. Japan also developed an "Intra-Vehicular Free-Flyer System" (IVFFS). And they introduced a "Space Humming Bird" (SHB) with a variable structural body to satisfy both safety and dexterity requirements. Its functions are very closed to PSA, but it has a unique design. The SHB is equipped with a robotic arm and a suction cup. Those can make it dock on the bulkhead and operate switches and panels [11]. Furthermore, an inter-vehicular flyer called Supplemental CAMera Platform (SCAMP) was developed in University of Maryland. The main experimental content is to hold the position and cross the designated flight path by using automatic control [12].

Attitude Control System (ACS) with high-precision and high-performance is required for the robot to move and work efficiently. There are plenty of attitude control methods applied to the space robot. From PD, PID control [13, 14], optimal control [15], adaptive control [16, 17] to robust control [18], they all have received good control results. But the dynamic model of the space robot system is multivariable strong coupling and nonlinear. This leads to that the control methods mentioned above have some disadvantages. For example, the PID control algorithm does not apply to the dynamic nonlinear systems. The optimal control algorithm has a weak robustness. The robust control system does not work at the best state. This reduces the steady-state accuracy of the system. The most popular robust control method called H_∞ has also a problem that its controller's order is too high. As typical intelligent control methods, the sliding mode control [19], fuzzy control and neural network control are effective tools for controlling system, and have achieved wide applications in space robotics. Zou *et al*. used terminal sliding mode and Chebyshev neural network to solve the finite-time attitude tracking control for spacecraft [20]. Gao *et al*. used fuzzy algorithm to control the CAS rover arm [21]. Liu and Li used the adaptive neural fuzzy control for mobile manipulators [22]. In this paper, PID Neural Network will be utilized to control a Space Station Astronaut Assisted Robot (SSAAR).

2. DESIGN OF THE SPACE STATION ASTRONAUT ASSISTED ROBOT SYSTEM

Based on the required tasks to assist astronauts' works and existed typical inter-vehicular floating robots, a space station astronaut assisted robot is designed. It can float in the space cabin and use its own control system to flight autonomously or hold position. In addition, it also has a certain degree of environmental awareness and intelligent capabilities. Thus, the robot can assist astronauts to complete some special scientific experiments or technical tests. Its functions are: (a) Positioning and navigation: The robot is equipped with binocular vision system that can achieve the functions of the environmental perception and 3D modeling, which can make the robot locate and navigate in the cabin. (b) Autonomous movement: The robot has a healthy position and attitude control system, which can make the robot 6-DOF flight autonomously and float in the cabin. (c) Remote control: Astronauts and ground staff control the robot via wireless transmission in the space station and on the ground respectively to accomplish specific tasks. (d) Autonomous monitoring: The robot has superior intelligence and able to carry out regular inspections and monitoring. Those can eliminate much of the workload of astronauts. (e) Health Management: The robot can be equipped with a temperature sensor, humidity sensor or pressure sensor and detect the cabin environment. These data can be transferred to the host computer and be observed and analyzed by the astronauts.

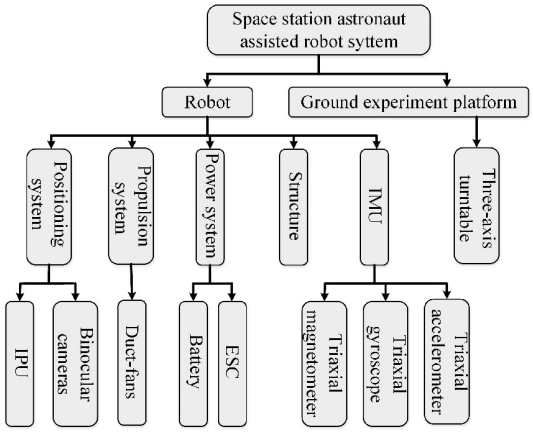

Fig. 1. A general structure of the space station astronaut assisted robotic system.

The space station astronaut assisted robotic system is composed of a float robot and the experimental platform, as shown in Fig. 1. The parts of the structure are introduced as follows.

2.1. Mechanical design

The ultimate goal and design idea for the space station astronaut assisted robotic structural scheme are meeting the demands. Through the research and analysis to the existed typical inter-vehicular floating robots and combined with the actual needs of the robot, the design requirements of the space station astronaut assisted robot are proposed as follows.

Based on the security and locomotive ability, the robot's shape is intended to be spherical. The dimension of the radius should be less than 300 mm. The weight should be less than 5 kg and the load capacity should be greater than 0.5 kg. (b) The robot should achieve six-degree-of-freedom movement in microgravity environment and

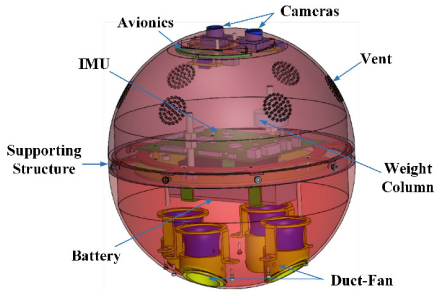

Fig. 2. A 3D model of the SSAAR.

Table 1. The technical parameters of the SSAAR.

Parameter	Technical Indicator
Diameter	250 mm
Weight	3 kg
Power	Battery, working time/one time charge > 0.5 h
Straight-line Speed	Max speed: $V_{\max} = 0.75\ m/s$
Rotational Speed	Max speed: $W_{\max} = 60^{\circ}/s$
Rotational Inertia	$I_x = 0.055\ kg \cdot m^2$ $I_y = 0.057\ kg \cdot m^2$ $I_z = 0.110\ kg \cdot m^2$

have a long flight time. (c) The structure can effectively protect the propellers and sensors to avoid collision damage. (d) The structure should have a moral symmetry that can avoid deflection or imbalance during the robots movement. (e) The robot can effectively reduce the external vibration and its own vibration.

Based on those mentioned above, a novel, ducted and spherical robot which can freely fly in the microgravity environment is proposed in this paper. The 3D model of the internal frame structure is shown in Fig. 2.

The robot is mainly composed of an external spherical shell and an internal frame structure. The spherical shell is made of metallic material and includes episphere and hyposphere. The connection of the episphere and hyposphere is matched with recesses and projections. Wire thread insertations are installed at the holes in the upper part of the episphere. The two hemispheres are linked together to form a ball by using screws. The internal structure is mainly composed of duct-fans propulsion module, Inertial Measurement Unit (IMU), avionics and binocular cameras.

The technical parametric indicators of the space station astronaut assisted robot are shown in Table 1.

2.2. Propulsion system

The propulsion system is a key part of the robot during flight in the cabin. At present, foreign inter-vehicular robots' propulsion systems mostly use the methods of

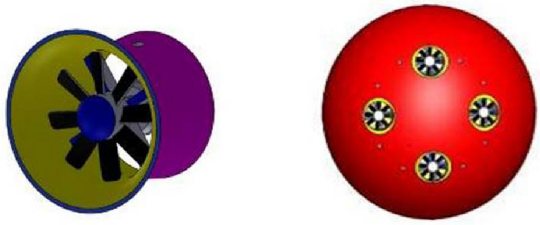

(a) A ducted fan model. (b) Ducted fans distribution diagram.

Fig. 3. Propulsion system of SSAAR.

high-pressure gas propulsion (eg SPHERES) and ducted fan propulsion (eg PSA, SHB and SCAMP). Considering about that the propulsion using high-pressure CO_2 or N_2 is easily contaminated in inter-vehicular environment and it is more troublesome to replace gas, so the ducted fan is chosen as the propulsion model of the space station astronaut assisted robot.

The ducted fan model is expressed in Fig. 3(a). Its advantages are: (a) Because the tip of fan is restricted by the duct, the impulsive noise and induced drag are reduction, and the efficiency is higher. (b) Under the same power consumption, the ducted fan will produce more thrust than the isolated propeller which has the same diameter with the ducted fan. (c) Because of the function of ducted ring, it has a compact structure, low aerodynamic noise and good safety.

The propulsion system of the space station astronaut assisted robot has totally four ducts. Each duct parallels to others and the four ducts are evenly distributed at the back of the robot (Fig. 3(b)). It can make the robot move in the microgravity environment at 6 DOF. Ducted fans are built inside the spherical shell. This will enhance the safety of the robot. Due to the thin spherical shell, ducted fasteners ensure the ducts more stable and reliable. Ducted fasteners are connected with the spherical shell through bolts and nuts, and the ducts are pressed firmly. Ducts would produce a slight vibration in high-speed rotation, so the locked nuts are chosen to prevent the nuts off.

2.3. Positioning system

The positioning mode of the space station astronaut assisted robot uses binocular visual image positioning system. This positioning mode uses two COMS cameras to positioning. For a feature point in the environment, two cameras are fixed on the front of the robot (Fig. 4) to capture the image of the point and to get the coordinates of the point respectively. As long as the exact relative position in two cameras is acquired, the point's coordinate in the coordinate system of a specified camera can be obtained through geometric method. That is to say the position of the feature point is determined [23].

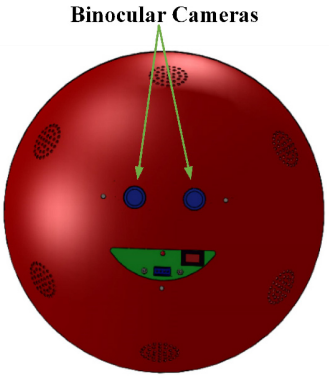

Fig. 4. Binocular cameras distribution diagram.

The binocular visual image positioning system obtains the exact position of the robot through the image analysis processing and image measurement. Then, the robot position coordinates in the cabin are calculated and provided for the robot to locate or plan trajectory.

2.4. IMU

To measure accurately the real-time attitude of the robot, a whole IMU sensor is designed. It can measure the attitude angles, angular velocities and angular accelerations of the robot in real time [24].

In Fig. 5, in order to improve the measurement accuracy, the IMU should be installed at the center of gravity of the space station astronaut assisted robot and remained levely with the support frame. Three axis directions are lined out in Fig. 5. The IMU is fixed upon the support frame, battery and ESC dead plate is connected below the support frame through coppers. Battery and ESC are installed up and down the dead plate through fasteners. At the same time, they are isolated by pillars to dissipate heat.

IMU sensory module physical map is shown in Fig. 6. It consists of the following components: (a) MCPU STM32; (b) Triaxial magnetometer; (c) Triaxial gyro; (d) Triaxial accelerometer; (e) Wireless communication module; (f) LCD. The real-time attitude data of the space station astronaut assisted robot are collected through the triaxial magnetometer, the triaxial gyro and the triaxial accelerometer (triaxial magnetometer measures attitude angles, the triaxial gyro measures angular velocities and the triaxial accelerometer measures angular accelerations). Then, the MCPU takes the collected data for data fusion through Kalman filter and calculates the Euler angles to get the robot's real-time attitude. Finally, attitude information will be transferred to the host computer for observation and analysis through wireless module.

2.5. Three-axis turntable for ground experiments

Because there is no microgravity environment in terrestrial experiments, the experimental device which can simulate microgravity experimental environment is needed in order to assist the robot's motion. The three-axis turntable is designed to assist the robot's attitude motion tests, which is illustrated in Fig. 7. It includes an outer ring, an inner ring and two spindles. The robot connects with the inner ring through spindles. The robot can do 3-DOF attitude motions in terms of pitch, roll and yaw respectively on the three-axis turntable assembly diagram as shown in

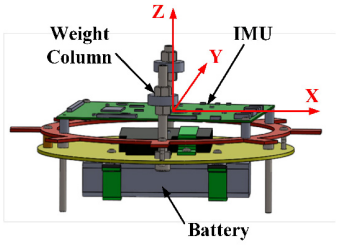

Fig. 5. IMU and power module model diagrams.

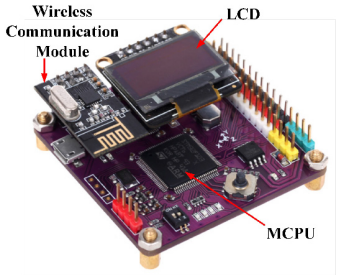

Fig. 6. IMU hardware.

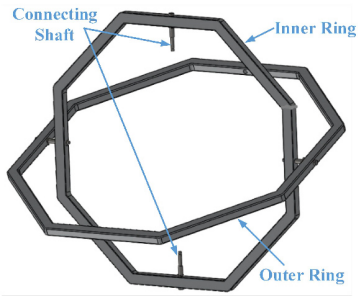

Fig. 7. Three-axis turntable model diagram.

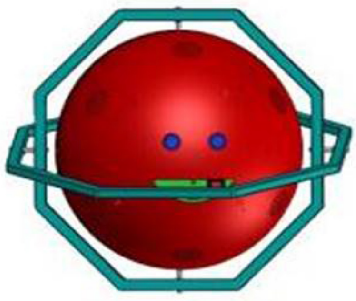

Fig. 8. Robot and turntable assembly diagram.

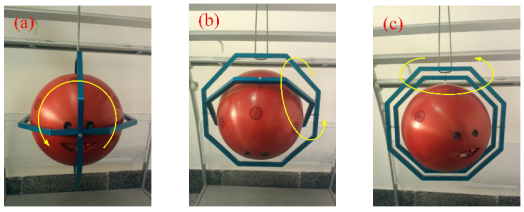

(a) Roll. (b) Pitch. (c) Yaw.

Fig. 9. Attitude control experimental platform.

Fig. 8.

The suspension method is invoked as the approach of simulating the microgravity environment. The suspension method is mainly balancing the robot's gravity through vertical tension of hang spring. The advantages include simple structure, easy to implement, and unlimited test time. So it is used extensively. Its drawbacks are that the truss mechanism which supports rope is complex, the space is large and rope follower mechanism commonly uses mechanical bearings. This will cause the motion friction large and seriously affect the accuracy of experiments. Based on those, the suspension method is only used for testing three-degree-of-freedom attitude control of the robot. The robot's position control will be finished on the air-floating platform in our further work. The specific experimental attitude control method is that installing the robot on the three-axis turntable and using the hang spring to hang the robot and turntable and make the robot balance in the air. The experimental method is shown in Fig. 9. The attitude control of the robot will be further studied in theory and simulations.

3. THE SPACE STATION ASTRONAUT ASSISTED ROBOT DYNAMICS MODELING

Dynamic modeling of the space station astronaut assisted robot is a prerequisite for the simulation experiments. Accurate dynamic model can provide reliable support for the design of the robot's attitude controller [25]. The attitude control of the robot has three input forces (rolling force, pitching force, yawing force) and three state outputs (roll, pitch, yaw), so it belongs to Multiple Input Multiple Output (MIMO) system. In this paper, the robotic model is explored in theory. And according to Newton - Euler equations, the performance parameters and characteristics of the actual system are given in simple and comprehensive by using a simplified set of mathematical expressions.

3.1. Movement principle

The robot changes the thrusts of four ducts by adjusting the ducted fans' speeds to meet its attitude control. In Fig. 11, X is the yaw axis, Y is the pitch axis, Z is the roll axis and the positive direction of Z is the forward direction of the robot. Fans of Th1 and Th3 are counterclockwise rotation, and the fans of Th2 and Th4 are clockwise rotation. When the four duct-fans' speeds are equal, their provided thrusts are equal, and the attitude of the robot would remain stable. On this basis, the robot attitude control principle is as follows:

1) Rolling motion: As shown in Fig. 10(a), on the basis of stable attitude of the robot, the fans speeds of Th1 and Th3 rise (or fall), while the fans speeds of Th2 and Th4 fall (or rise). The reaction torques of Th1 and Th3 are bigger than the reaction torques of Th2 and Th4. So the robot can rotate around Z affected by surplus reaction torque, and the direction is opposite to the directions of Th1 and Th3. Thus, the rolling motion of the robot can be achieved.

2) Pitching motion: As shown in Fig. 10(b), on the basis of stable attitude of the robot, the fans speeds of Th2 and Th4 remain unchanged. Increase (or decrease) the fan speed of Th3, while decrease (or increase) the fan speed of Th1. And the amount of changes of fans speeds Th1 and Th3 are equal. Thus, the robot can rotate around Y and the pitching motion of the robot can be achieved.

3) Yawing motion: As shown in Fig. 10(c), similar to pitching motion, the fans speeds of Th1 and Th3 remain unchanged, and the fans speeds of Th2 and Th4 are changed. Thus, the robot can rotate around X and the yawing motion of the robot can be achieved.

3.2. Coordinate system and attitude matrix

The motional principle of the space station astronaut assisted robot can be simplified as shown in Fig. 11. Its attitude needs to associate with the earth coordinate system and the body coordinate system. In order to describe the attitude motion state of the robot accurately, an appropriate coordinate system is needed in order to establish firstly [25].

The earth coordinate system $(O_E X_E Y_E Z_E)$: Define a designated point on the earth as the origin, define a horizontal plane as $X_E O_E Y_E$, define a fixed direction (the direction is east generally) as X_E positive direction, define its 90° counterclockwise direction (the direction is north generally) as Y_E positive direction, and define the vertical upward direction as Z_E positive direction. The establishment of the whole coordinate system is consistent with the right-hand rule. Such coordinate system is also called 'NEU (North East Up coordinate system)' in inertial navigation. The coordinate system is attached on the ground. In small-area space description, the curvature of the ground can be taken into account to approximate the ground to a plane. Thus, it can simplify the robot's attitude motion.

The body coordinates system $(O_B X_B Y_B Z_B)$: As shown in Fig. 12, the origin O_B of the body coordinate system is on the robot's center of gravity (center of the sphere). Set the line which passes O_B and parallel to the connection

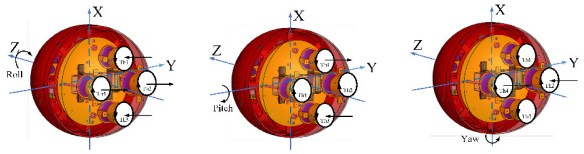

(a) Roll. (b) Pitch. (c) Yaw.

Fig. 10. Motion schematics.

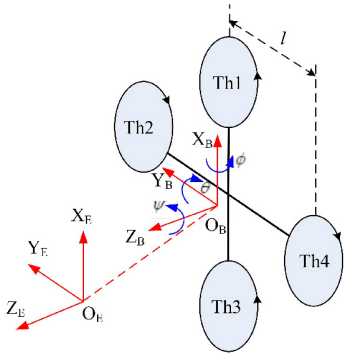

Fig. 11. Coordinate system schematic.

of Th1 and Th3 as X_B, and the direction of Th3 to Th1 is the positive direction. Set the line which passes O_B and parallel to the connection of Th2 and Th4 as Y_B, and the direction of Th4 to Th2 is the positive direction. Define the line which passes OB and is perpendicular to $X_BO_BY_B$ as Z_B, and the robot's forward hemisphere direction is the positive direction of Z_B.

As shown in Fig. 12, the space attitude can be seen as the composite effect of making basic rotation around Z_E, Y_E and X_E successively.

The corresponding transformation matrices of basic rotations are:

$$R(X_E,\phi)=\begin{bmatrix}1 & 0 & 0\\ 0 & \cos\phi & \sin\phi\\ 0 & -\sin\phi & \cos\phi\end{bmatrix}, \tag{1}$$

$$R(Y_E,\theta)=\begin{bmatrix}\cos\theta & 0 & \sin\theta\\ 0 & 1 & 0\\ -\sin\theta & 0 & \cos\theta\end{bmatrix}, \tag{2}$$

$$R(Z_E,\psi)=\begin{bmatrix}\cos\psi & -\sin\psi & 0\\ \sin\psi & \cos\psi & 0\\ 0 & 0 & 1\end{bmatrix}. \tag{3}$$

The transformation matrix is:

$$\begin{aligned}C_B^E &= R(X_E,\phi)R(Y_E,\theta)R(Z_E,\psi)\\ &=\begin{bmatrix}c\theta c\psi & -c\theta s\psi & s\theta\\ -s\phi s\theta c\psi+c\phi s\psi & s\phi s\theta s\psi+c\phi c\psi & s\phi c\theta\\ -c\phi s\theta c\psi-s\phi s\psi & c\phi s\theta s\psi-s\phi c\psi & c\phi c\theta\end{bmatrix},\end{aligned} \tag{4}$$

where 's' represents sin and 'c' represents cos.

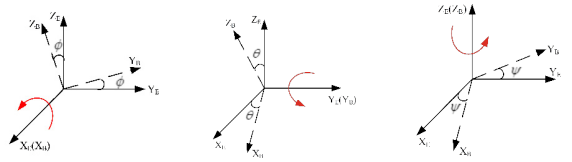

(a) Yaw angle ϕ. (b) Pitch angle θ. (c) Roll angle ψ.

Fig. 12. Basic rotation schematic.

3.3. The mechanical model of the space station astronaut assisted robot

The space station astronaut assisted robot achieves the attitude control by changing the thrusts of four duct-fans.

As shown in Fig. 13, F_i $(i=1,2,3,4)$ is the air force generated by each duct-fan's work, $T_{i,c}$ $(i=1,3)$ is reaction torque generated by resistance when the duct-fan rotates counterclockwise, and $T_{i,n}$ $(i=2,4)$ is reaction torque generated by resistance when the duct-fan rotates clockwise. According to aerodynamics [26], the following formulas can be derived.

$$F_i = k_F\omega_i^2 \qquad (i=1,2,3,4), \tag{5}$$

$$T_{i,c} = k_{T,c}\omega_i^2 \qquad (i=1,3), \tag{6}$$

$$T_{i,n} = k_{T,n}\omega_i^2 \qquad (i=2,4), \tag{7}$$

where k_F is the thrust coefficient of the ducts, $k_{T,c}$ is the torque coefficient of duct-fan counterclockwise rotation, $k_{T,n}$ is the torque coefficient of duct-fan clockwise rotation, and $k_{T,c}=-k_{T,n}$, ω_i is the speed of the i-th fan.

The attitude of the robot is closely related to the torques of three angles.

Rolling torque:

$$T_\psi = T_{1,c}+T_{2,n}+T_{3,c}+T_{4,n} \tag{8}$$

Pitching torque:

$$T_\theta = (F_3-F_1)l \tag{9}$$

Yawing torque:

$$T_\phi = (F_4-F_2)l, \tag{10}$$

where l is the vertical distance between the axis of duct-fan and the axis of the robot's center of gravity.

3.4. The dynamic model of the space station astronaut assisted robot

The dynamic model of the space station astronaut assisted robot is established based on the mechanical model. The attitude dynamic model is obtained through the analysis of rigid body dynamics via Newton - Euler equation [27].

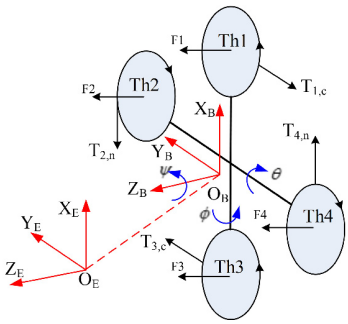

Fig. 13. Locomotion diagram of the robot.

$$\begin{cases} \dot{\phi} I_x = \dot{\theta}\dot{\psi} I_y - I_z + \left(T_\phi + T_{\phi cor} + T_{\phi d} - k_\phi \dot{\phi} l\right) \\ \dot{\theta} I_y = \dot{\phi}\dot{\psi} I_z - I_x + \left(T_\theta + T_{\theta cor} + T_{\phi d} - k_\theta \dot{\theta} l\right) \\ \dot{\psi} I_z = \dot{\phi}\dot{\theta} I_x - I_y + \left(T_\psi + T_{\psi cor} + T_{\psi d} - k_\psi \dot{\psi} l\right), \end{cases} \tag{11}$$

where I_x, I_y, I_z are rotational inertias around X_B, Y_B and Z_B, respectively. $T_{\phi cor}$, $T_{\theta cor}$, $T_{\psi cor}$ are the torques of Coriolis forces on three axis, respectively. $T_{\phi d}$, $T_{\theta d}$, $T_{\psi d}$ are disturbing torques on three axis, respectively. k_ϕ, k_θ, k_ψ are air resistance coefficients on the triaxial rotational directions, respectively.

Set the robot's control inputs as U_1, U_2, U_3, which express the resultant torques on roll, pitch and yaw directions, respectively. That is

$$\begin{cases} U_1 = T_{1,c} + T_{2,n} + T_{3,c} + T_{4,n} \\ U_2 = F_3 - F_1 \\ U_3 = F_4 - F_2. \end{cases} \tag{12}$$

Based on the experiments made in the microgravity environment of space, the disturbing torques, Coriolis forces and air resistances can be ignored. So the attitude dynamic model can be simplified as follows according to formula (8) to formula (12).

$$\begin{cases} \ddot{\phi} = \dot{\theta}\dot{\psi}\left(\dfrac{I_y - I_z}{I_x}\right) + \dfrac{l}{I_x} U_3 \\ \ddot{\theta} = \dot{\phi}\dot{\psi}\left(\dfrac{I_z - I_x}{I_y}\right) + \dfrac{l}{I_y} U_2 \\ \ddot{\psi} = \dot{\phi}\dot{\theta}\left(\dfrac{I_x - I_y}{I_z}\right) + \dfrac{1}{I_z} U_1 \end{cases} \tag{13}$$

From system dynamic model, it can be known that pitch channel is controlled by Th1 and Th3, yaw channel is controlled by Th2 and Th4, and roll channel is controlled by four ducts together.

4. DESIGN OF PIDNN ATTITUDE CONTROLLER

In recent years, with the research and application of the neural network in the field of space robot, researchers begin to use the neural network to combine with PID for improving the performance of traditional PID control method. Nowadays, the proposed methods of combing neural network with PID can be summarized in two types: 1) PID controller with single neuron structure [28]; 2) Using the neural network to determine the PID parameters [30, 31]. But both of the methods have their shortcomings. One of the shortcomings is that using the neural network to determine the PID parameters leads to a complex structure and large computational costs. And another shortcoming is that it cannot avoid the weaknesses that the conventional neural networks have. For example, its convergence speed is slow, it's easy to fall into a local minimum, and it's difficult to determine the number of hidden layers and the initial connection weights. The structure of the PID controller with single neuron structure is simple. It's easy to implement, and it has some advantages that the neural networks have. However, it also has the essential weaknesses. On one hand, it is still a method of selecting the PID controller parameters. On the other hand, this single-layer network has only linear classification capability, and it is difficult to achieve good performance for controlling complex systems. The control effects of two methods are not good in the MIMO system. The current research results are mainly found at some SISO systems.

PIDNN (PID Neural Network) is not the simple combination of neural network and traditional PID, and not selection and adjustment to the PID parameters using neural network. The basis of PIDNN is to define the neurons which have the functions of proportional, integral and differential respectively to integrate the PID control law into the neural network [28, 29]. The robot is a MIMO and nonlinear system, this control method has both the advantages of PID and the advantages of neural network, and is especially suitable for MIMO system. So, the PIDNN is chosen to design the attitude controller of the space station astronaut assisted robot.

4.1. The structure of PIDNN attitude controller

The designed PIDNN attitude controller is shown in Fig. 14. From Fig. 14, it can be seen that the controller

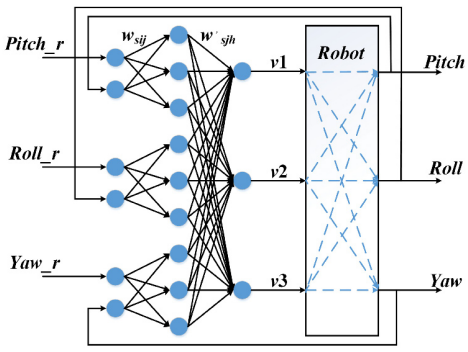

Fig. 14. PIDNN attitude controller structure diagram.

has three inputs and three outputs. It is composed of three 2×3×1 subnets crossing in parallel to constitute a forward network with three layers. This makes up a network with 6×9×3 structure whose input layer has 6 input neurons, hidden layer has 9 processing neurons (including 3 proportional neurons, 3 integral neurons and3 differential neurons) and output layer has 3 output neurons. The input layer to the hidden layer is independent in accordance with the subnets. While the hidden layer to the output layer is cross-connected to each other. This makes the whole PIDNN into one. The input layer is put into 3 given attitude angles (*Pitch_r, Roll_r, Yaw_r*) and 3 measurement attitude angles (*Pitch, Roll, Yaw*). And the output layer as the outputs of the controller to complete the decoupling control work.

4.2. The forward algorithm of the PIDNN attitude controller

At any sampling time k, the forward algorithm of PIDNN is shown as follows.

1) Input layer

The input layer has 6 neurons. Its relationship of input and output is

$$x_{si}(k) = u_{si}(k), \tag{14}$$

where u_{si} ($i = 1, 2$) is the input value of the input layer neuron, x_{si} ($i = 1, 2$) is the output value of the input layer neuron, and s ($s = 1, 2, 3$) is the number of parallel network.

2) Hidden layer

The hidden layer contains 9 neurons which are 3 proportional neurons, 3 integral neurons and 3 differential neurons. Their formulas of input total value are

$$u_{sj}^{'}(k) = \sum_{j=1}^{2} \omega_{sij} x_{si}(k). \tag{15}$$

The hidden layer neurons have three kinds of state functions. When the output value is limited, the output of proportional neuron is

$$x_{s1}^{'}(k) = u_{s1}^{'}(k). \tag{16}$$

The output of integral neuron is

$$x_{s2}^{'}(k) = x_{s2}^{'}(k-1) + u_{s2}^{'}(k). \tag{17}$$

The output of differential neuron is

$$x_{s3}^{'}(k) = u_{s3}^{'}(k) - u_{s3}^{'}(k-1). \tag{18}$$

In (15)-(18), s ($s = 1, 2, 3$) is the number of parallel network, j ($j = 1, 2, 3$) is the number of hidden layer neuron in the subnets, and ω_{sij} is connection weight of input layer to the hidden layer in each subnet, superscript ' means the hidden layer value.

3) Output layer

The output layer of PIDNN has 3 neurons which form 3-dimensional output. The input of each output neuron is the weighted sum of all output values of hidden layer neurons.

$$u_h^{''}(k) = \sum_{s=1}^{3}\sum_{j=1}^{3} \omega_{sjh}^{'} x_{sj}^{'}(k) \tag{19}$$

The output of the output layer is

$$v_h(k) = x_h^{''}(k) = u_h^{''}(k). \tag{20}$$

In (19) and (20), h ($h = 1, 2, 3$) is the number of output layer neuron, $\omega_{sjh}^{'}$ is the connection weight of hidden layer to the output layer in each subnet, superscript '' means the output layer value.

4.3. The back propagation algorithm of the PIDNN attitude controller

The back propagation algorithm of PIDNN attitude controller considers PIDNN and the robot attitude system as a whole generalized network, and the robot attitude system becomes the last layer of the network. This generalized network uses batch learning algorithm with the error backward propagation. And the aim of learning is to make

$$\begin{aligned} J &= \sum_{s=1}^{3} E_s \\ &= \frac{1}{l}\sum_{s=1}^{3}\sum_{k=1}^{l} [r_s(k) - y_s(k)]^2 \\ &= \frac{1}{l}\sum_{s=1}^{3}\sum_{k=1}^{l} e_s^2(k) \end{aligned} \tag{21}$$

minimum. In (21), l is the number of sampling points in each batch, k is the sampling point. The weighs through n_0-step training and learning are determined by the following formulas.

1) The weights of hidden layer to output layer

The iterated function of hidden layer to output layer's weights is

$$w_{sjh}^{'}(n_0+1) = w_{sjh}^{'}(n_0) - \eta_{sjh}^{'} \frac{\partial J}{\partial w_{sjh}^{'}}. \tag{22}$$

Because there are coupling functions between the outputs and inputs of multi-variable object, we have

$$\frac{\partial J}{\partial w_{sjh}^{'}} = \sum_{s=1}^{3} \frac{\partial J}{\partial E_s} \times \frac{\partial E_s}{\partial y_s} \times \frac{\partial y_s}{\partial v_h} \times \frac{\partial v_h}{\partial x_h^{''}} \times \frac{\partial x_h^{''}}{\partial u_h^{''}} \times \frac{\partial u_h^{''}}{\partial w_{sjh}^{'}}. \tag{23}$$

2) The weights of input layer to hidden layer

The iterated function of input layer to hidden layer's weights is

$$w_{sij}(n_0+1) = w_{sij}(n_0) - \eta_{sij}\frac{\partial J}{\partial w_{sij}}, \tag{24}$$

where

$$\frac{\partial J}{\partial w_{sij}} = \sum_{s=1}^{3}\left[\frac{\partial J}{\partial E_s}\times\frac{\partial E_s}{\partial y_s}\left(\sum_{h=1}^{m}\frac{\partial y_s}{\partial v_h}\times\frac{\partial v_h}{\partial w_{sij}}\right)\right], \tag{25}$$

$$\frac{\partial v_h}{\partial w_{sij}} = \frac{\partial v_h}{\partial x_h''}\times\frac{\partial x_h''}{\partial u_h''}\times\frac{\partial u_h''}{\partial x_{sj}'}\times\frac{\partial x_{sj}'}{\partial u_{sj}'}\times\frac{\partial u_{sj}'}{\partial w_{sij}}. \tag{26}$$

In the above formulas, s ($s = 1, 2, 3$) is the serial number of the parallel subnets, i ($i = 1, 2$) is the serial number of the subnet's input neurons, j ($j = 1, 2, 3$) is the serial number of the subnet's hidden neurons, h ($h = 1, 2, 3$) is the serial number of the output neurons, x is the input value of each layer neurons, u is the output value of each layer neurons, v is the input value of the robot dynamic model, y is the output value of the robot dynamic model, r is the given input value of the whole system, ω_{sij} is the connection weight of the input layer to the hidden layer, and ω_{sjh}' is the connection weight of the hidden layer to the output layer.

5. SIMULATION

In order to verify PIDNN controller, the simulation experiment is conducted. This paper uses *Adams* which is a mechanical dynamics simulation software to design the virtual mechanical model of the robot. Then, the *Matlab/Simulink* is used to build up the control system simulation platform. Finally, the rationality of the designed robot's structural dynamics and the control effect of PIDNN controller are validated by conducting the dynamics co-simulation [32, 33].

5.1. Dynamics simulation of the robotic system using *Adams*

First of all, the robot physical model is built up by using *Soildworks* software as shown in Fig. 15. The space station astronaut assisted robot system includes a robot and a three-axis turntable. The robot structure includes a body composed by two hemispheres, a pair of binocular cameras and a circuit board, four duct-fan propulsion systems etc. It can achieve three-degree-of-freedom motions in terms of pitch, roll and yaw, respectively.

We put the robot system 3D structural model built in *Solidworks* to *Adams*, edit the property of each component and define the related properties such as quality, material and the rotational inertia. Thus, the virtual model will have the similar physical characteristics with the actual model. And the kinematics and dynamics simulation of the robot can be obtained by *Adams* as shown in Fig. 16.

Table 2. The conversions of the robot system's forces and torques.

Name	Variable	Function
Force of Th1	*Force1*	SQRT(VARVAL(.Robot .Speed1))*0.1188
Force of Th2	*Force2*	SQRT(VARVAL(.Robot .Speed2))*0.1188
Force of Th3	*Force3*	SQRT(VARVAL(.Robot .Speed3))*0.1188
Force of Th4	*Force4*	SQRT(VARVAL(.Robot .Speed4))*0.1188
Torque of Th1	*Torque1*	SQRT(VARVAL(.Robot .Speed1))*0.0036
Torque of Th2	*Torque2*	SQRT(VARVAL(.Robot .Speed2))*0.0036
Torque of Th3	*Torque3*	SQRT(VARVAL(.Robot .Speed3))*0.0036
Torque of Th4	*Torque4*	SQRT(VARVAL(.Robot .Speed4))*0.0036

We define the rotational constraints in four duct-fans' centers, define spherical hinge in the center of the spherical body, define the rotational constraints on the four shafts, define a fixed constraint between the outer ring of the three-axis turntable and the ground, and define fixed constraints on the other parts that have no relative motion. At the same time, define rotational drives and linear drives at the four duct-fans as driving torques and driving forces of the fan-ducts. The forces and torques are obtained by the conversions of functions as shown in Table 2.

To achieve data transfer between mechanical systems and control systems, the parameter variables need to be set. We build up 7 state variables in *Adams* including 4 speed variables of duct-fans and 3 Euler angle variables expressed the robot's attitude, which are shown in Table 3.

Use the model of *Adams/Control* to generate the robot attitude subsystem model which can conduct the co-simulation with *Matlab* by setting parameters as shown in Fig. 17. It includes 4 input variables (*Speed1, Speed2, Speed3, Speed4*) and 3 output variables (*ROLL, PITCH,*

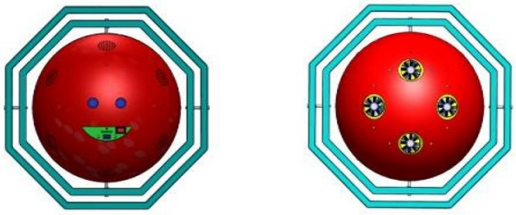

(a) Front view. (b) Rear view.

Fig. 15. A 3D model of the robot.

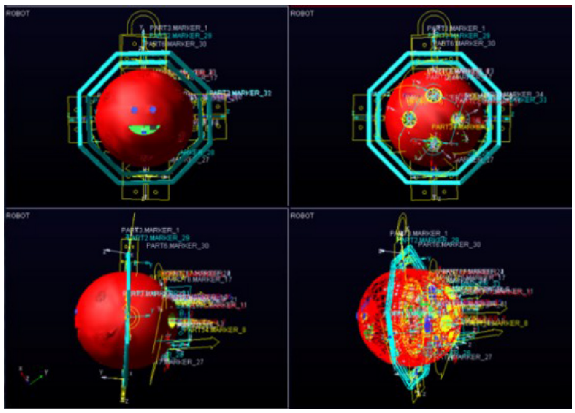

Fig. 16. Robot model in *Adams*.

Table 3. Parameter variables of the robot system.

Name	Variable	Function
Speed of Th1	*Speed1*	F(time,...)=0
Speed of Th2	*Speed2*	F(time,...)=0
Speed of Th3	*Speed3*	F(time,...)=0
Speed of Th4	*Speed4*	F(time,...)=0
Roll angle	*ROLL*	F(time,...)=AZ(.Robot.PART2 .MARKER_1, .Robot.ground.MARKER_4)
Pitch angle	*PITCH*	F(time,...)=AY(.Robot.PART2 .MARKER_1, .Robot.ground.MARKER_4)
Yaw angle	*YAW*	F(time,...)=AX(.Robot.PART2 .MARKER_1, .Robot.ground.MARKER_4)

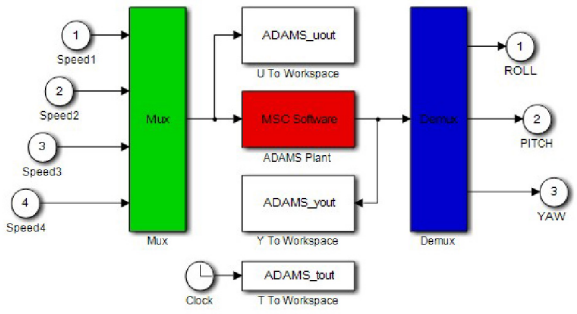

Fig. 17. Robot attitude subsystem in co-simulation.

YAW). The data transfer between *Adams* and *Matlab* can be achieved through this model. As shown in Fig. 18, *Adams* calls speed variable values of the control system outputs in time, and make them as the duct-fans' speed values of that moment. While, each Euler angle variable of the robot also can feed back to the control system in real time. This can make up the closed-loop attitude control system and achieve the accuracy control.

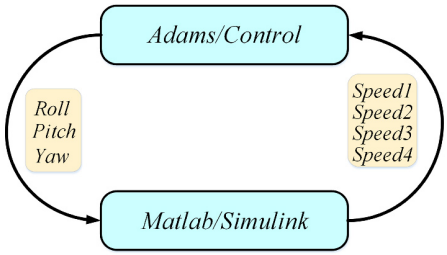

Fig. 18. . Data transfer of co-simulation system.

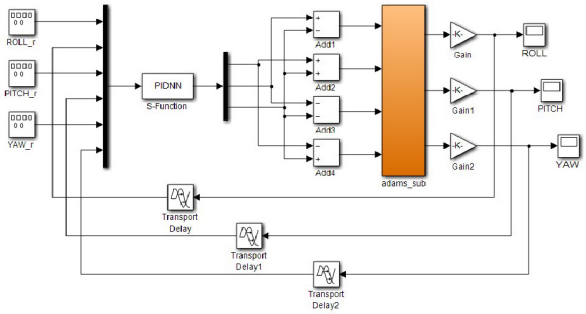

Fig. 19. Simulation of PIDNN attitude control system.

5.2. The simulation of PIDNN attitude controller

The simulation of PIDNN uses *Simulink* model and *S* function in *Matlab* to complete together. Fig. 19 gives the simulation model of this control system. From this figure it can be seen that the PIDNN controller has 6 inputs, those are the given value of each channel (*ROLL_r, PITCH_r, YAW_r*) and the feedback output of each channel (*ROLL, PITCH, YAW*). The output is duct-fan's speed valuation corresponding attitude angle.

In order to achieve the map of $(r_i, y_i) \to e_i$, choose the initial connection weights of the input layer to the hidden layer as $\omega_{s11} = 1$, $\omega_{s12} = -1$, $\omega_{s21} = 0.1$, $\omega_{s22} = -0.1$, $\omega_{s31} = 1$, $\omega_{s32} = -1$. That is

$$W_{ij} = \begin{bmatrix} 1 & -1 & 0 & 0 & 0 & 0 \\ 0.1 & -0.1 & 0 & 0 & 0 & 0 \\ 1 & -1 & 0 & 0 & 0 & 0 \\ 0 & 0 & 1 & -1 & 0 & 0 \\ 0 & 0 & 0.1 & -0.1 & 0 & 0 \\ 0 & 0 & 1 & -1 & 0 & 0 \\ 0 & 0 & 0 & 0 & 1 & -1 \\ 0 & 0 & 0 & 0 & 0.1 & -0.1 \\ 0 & 0 & 0 & 0 & 1 & -1 \end{bmatrix}, \quad (27)$$

where s means layer of neural network.

In order to balance several independent controllers when the neural network connection weights take the initial values, the connection weights initial values of the hidden layer to the output layer should be chosen as

$$\omega'_{s1h} = K_P, \quad \omega'_{s2h} = K_I, \quad \omega'_{s3h} = K_D.$$

That is

$$W_{jk} = \begin{bmatrix} K_{P\_Roll} & 0 & 0 \\ K_{I\_Roll} & 0 & 0 \\ K_{D\_Roll} & 0 & 0 \\ 0 & K_{P\_Pitch} & 0 \\ 0 & K_{I\_Pitch} & 0 \\ 0 & K_{D\_Pitch} & 0 \\ 0 & 0 & K_{P\_Yaw} \\ 0 & 0 & K_{I\_Yaw} \\ 0 & 0 & K_{D\_Yaw} \end{bmatrix}^{\mathrm{T}}, \quad (28)$$

where s ($s = 1, 2, 3$) means layer of neural network, h ($h = 1, 2, 3$) means the serial number of output neural network, K_P, K_I, K_D mean the coefficients of proportion, differentiation and integration of neuron control. K_P, K_I, K_D are adjusted in traditional PID controller.

The convergence of the PIDNN attitude control system depends on the selection of learning step size. Learning step size η represents the convergence rate. If η is too small, error fluctuation is small, but the learning rate is slow. While if the η is too large, the learning rate will be fast, this will cause the network swing and lead to the risk of non-convergence. So choosing a suitable η is important. In practical simulation, in order to simplify the calculation, the step size can take a small enough positive number firstly. In this paper, we take $\eta(0) = 0.01$, and then, the step size adjusted formula is

$$\eta(t) = \eta(t-1)\frac{J(t-1) - J(t)}{J(t-1) + J(t)}. \quad (29)$$

Equation (29) can adjust the step size. J is quadratic performance index.

The simulation firstly verifies the responsiveness of the designed PIDNN attitude controller under the step signal. The attitude angles are given 30° signals and input into the three channels of roll, pitch and yaw respectively. We can observe the step response curve by oscilloscopes. Then, the 30° given signals are input into the three attitude channels together, and also observe the step response curves and step response error curves. Through adjustment, take $K_{P-Roll} = 12.0$, $K_{I-Roll} = 0.2$, $K_{D-Roll} = 28.0$; $K_{P-Pitch} = 7.0$, $K_{I-Pitch} = 0.2$, $K_{D-Pitch} = 15.7$; $K_{P-Yaw} = 12.3$, $K_{I-Yaw} = 0.5$, $K_{D-Yaw} = 11.8$, and take the training step size $n_0 = 20$. The results are shown in Fig. 20. From Fig. 20, it can be known that under 30° step signal, the all three attitude channels reach a stable attitude eventually. When the signal acts alone, the overshoot of roll channel is 16.7% and the adjusting time is 2.0 s; the pitch channel has no overshoot and the adjusting time is 1.5 s; the overshoot of yaw channel is 13.3% and the adjusting time is 3 s. And when one of the channel acts, the other channels have a small coupling. When the three channels are acted together, the max overshoot is 16.7% and the adjusting time is 2.4 s. The increase of overshoot and adjusting is caused by the features of the robot dynamics model, and this leads to the three attitude channels not completely independent and a small amount of coupling. As we know, overshoot is an important indicator in dynamic performance of control system. It influences stability of the control system. The initial values of K_P, K_I, K_D can be adjusted to decrease the overshoot in each channel. The above results show that the designed PIDNN attitude controller can control the robot steadily to move

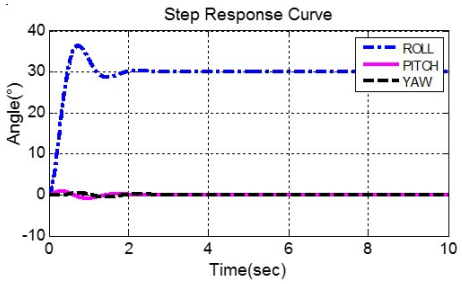

(a) Step response curve of roll angle.

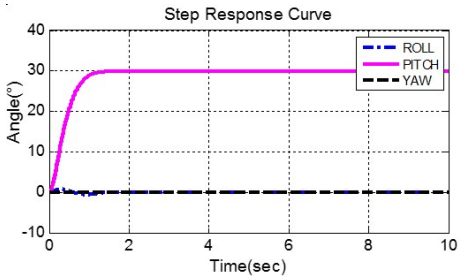

(b) Step response curve of pitch angle.

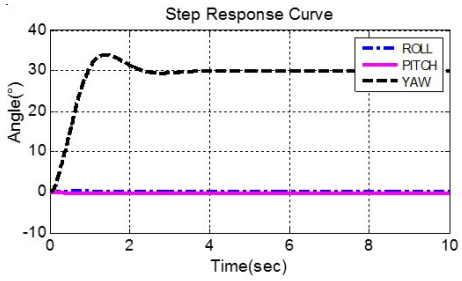

(c) Step response curve of yaw angle.

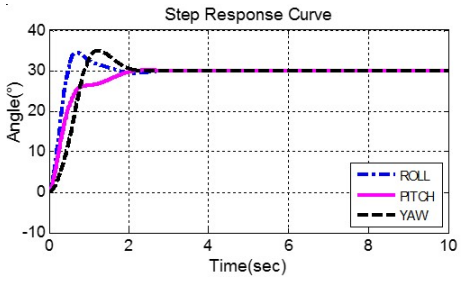

(d) Step response curves of the 3 channels.

Fig. 20. Step response curves of PIDNN attitude controller.

to the specified attitude in a short time under the action of the step signal.

To further verify the validity of the PIDNN attitude controller, the signal tracking simulation is needed to conduct. Firstly, we input a sinusoidal signal whose amplitude is 30° and cycle is 5 s into the three channels, those are roll, pitch and yaw respectively, and observe the signal tracking curves with oscilloscopes. Then, we input the same sinusoidal signal into the three channels together and also observe the tracking curves. The sine tracking curves are shown in Fig. 21.

It can be seen from the above figures that when the sinusoidal signal with amplitude of 30° and cycle of 5s is input into the three channels, they all can track the given signal well. When the sinusoidal signal acts alone, the max error of roll angle is 3°, the max error of pitch angle is 2° and the max error of yaw angle is 4°. And when one of the channels is acted, the others' couplings are almost zero. When the three channels are acted together, the roll channel can track the sinusoidal signal most accurately, the amplitude in pitch channel is slightly large and the amplitude in yaw channel is slightly small, but the max error is less than 5°. The above results show that the designed PIDNN attitude controller can control the robot track the attitude signal quickly, stably and accurately.

6. CONCLUSIONS AND FUTURE WORKS

In this paper, a space station astronaut assisted robot is designed according to the features of microgravity environment and the mission requirements of assisting astronauts. The structure, propelling system, positioning system and IMU of the robot and a three-axis turntable are designed. After manufacturing, the technical parameters of the entire model can all be matched. Then, the motion principle of the robot is analyzed to prove that the designed robot can achieve the six-degree-of-freedom motion in the microgravity environment. And the robot's dynamics equations are built up. Finally, the attitude controller of the space station astronaut assisted robot is realized by using PIDNN control algorithm. Then, the co-simulation of the robot's attitude control is made by using *Adams* and *Matlab/Simulink*. The simulation results show the effectiveness of the designed PIDNN attitude controller.

Based on our previous works [34–45], the following works are planned: (a) Physical experiments on the attitude control of the space station astronaut assisted robot to further validate the reasonableness of the robot and the effectiveness of the PIDNN attitude controller. (b) Study the six-degree-of freedom motion and test on the gas floating platform. (c) Based on the current researches, the spacecraft formation flying technology will be studied.

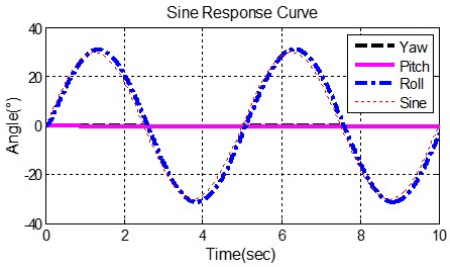

(a) Sine tracking curve of roll angle.

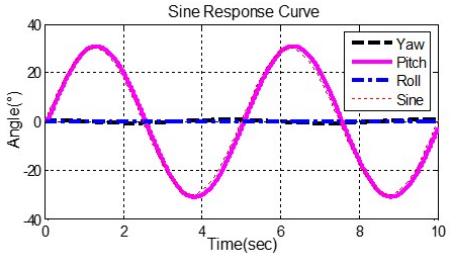

(b) Sine tracking curve of pitch angle.

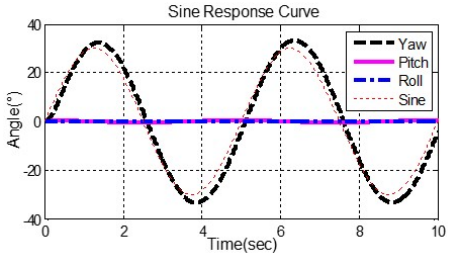

(c) Sine tracking curve of yaw angle.

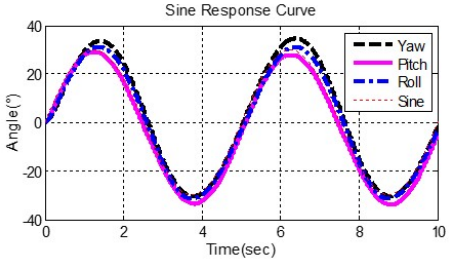

(d) Sine tracking curves of the 3 channels.

Fig. 21. Sine tracking curves of PIDNN attitude controller.

REFERENCES

[1] J. P. Zhou, "Chinese space station project overall vision," *China Manned Space Eng. Office*, vol. 19, no. 2, pp. 1-10, 2013.

[2] J. L. Zhao, S. Z. Yan, and J. N. Wu, "Analysis of parameter sensitivity of space manipulator with harmonic drive based on the revised response surface method," *Acta Astronautica*, vol. 98, pp. 86-96, 2014. [click]

[3] T. F. Yang, S. Z. Yan, and Z. Y. Han, "Nonlinear model of space manipulator joint considering time-variant stiffness and backlash," *J. Sound Vibration*, vol. 341, pp. 246-259, 2015. [click]

[4] A. Flores-Abad, O. Ma, K. Pham, and S. Ulrich, "A review of space robotics technologies for on-orbit servicing," *Progress in Aerospace Sci.*, vol. 68, pp. 1-26, 2014. [click]

[5] S. Nag, J. G. Katz, and A. Saenz-Otero, "Collaborative gaming and competition for CS-STEM education using SPHERES zero robotics," *Acta Astronautica*, vol. 83, pp. 145-174, 2013. [click]

[6] P. Acquatella, "Development of automation & robotics in space exploration," *Proc. of the AIAA SPACE Conf. & Expos.*, pp. 121-135, 2009.

[7] J. G. Liu, Y. M. Li, Y. Zhang, Q. Gao, and B. Zuo, "Dynamics and control of parallel mechanism for active vibration isolation in space station," *Nonlinear Dyn.*, vol. 76, no. 3, pp. 1737-1751, 2014. [click]

[8] G. A. Dorais and Y. Gawdiak, "The personal satellite assistant – An internal spacecraft autonomous mobile monitor," *IEEE Int. Conf. Aerospace*, pp. 333-348, 2003.

[9] A. S. Otero, A. Chen, and D. W. Miller, "SPHERES: Development of an ISS laboratory for formation flight and docking research," *IEEE Int. Conf. Aerospace*, pp. 59-73, 2002.

[10] G. J. Eslinger and A. Saenz-Otero, "Electromagnetic formation flight control using dynamic programming," *Proc. of 36th Annual AAS Guid. Control Conf.*, pp. 17-32, 2013.

[11] Y. Tsumaki and I. Maeda, "Intra-vehicular free-flyer with manipulation capability," *Adv. Robotics*, vol. 24, no. 3, pp. 343-358, 2010. [click]

[12] C. McGhan, R. L. Bebacca, R. M. Sanner, and E. M. Atkins, "Semi-autonomous inspection with a neutral buoyancy free-flyer," *Proc. of AIAA Guid., Navig., Control Conf.*, pp. 5483-8493, 2006.

[13] R. Varatharajoo, C. T. Wooi, and M. Mailah, "Two degree-of-freedom spacecraft attitude controller," *Adv. in Space Res.*, vol. 47, no. 4, pp. 685-689, 2011. [click]

[14] H. Bang, M. J. Tank, and H. D. Choi, "Large angle attitude control of spacecraft with actuator saturation," Control Eng. Prac., vol. 11, no. 9, pp. 989-997, 2003. [click]

[15] W. C. Luo, Y. C. Chu, and K. V. Ling, "Inverse optimal adaptive control for attitude tracking of spacecraft," *IEEE Trans. Autom. Control*, vol. 50, no. 11, pp. 1639-1654, 2005. [click]

[16] Z. Y. Chen and J. Huang, "Attitude tracking and disturbance rejection of rigid spacecraft by adaptive control," *IEEE Trans. Autom. Control*, vol. 54, no. 3, pp. 600-605, 2009. [click]

[17] W. C. Cai, X. H. Liao, and D. Y. Song, "Indirect robust adaptive fault-tolerant control for attitude tracking of spacecraft," *J. Guid., Control, Dyn.*, vol. 31, no. 5, pp. 1456-1463, 2008.

[18] D. Bustan, S. K. H. Sani, and N. Pariz, "Immersion and invariance based fault tolerant adaptive spacecraft attitude control," *Int. J. Control, Autom. Syst.*, vol. 12, no. 2, pp. 333-339, 2014. [click]

[19] B. Xiao, Q. Hu, and Y. Zhang, "Adaptive sliding mode fault tolerant attitude tracking control for flexible spacecraft under actuator saturation," *IEEE Control Syst. Techn.*, vol. 20, no. 6, pp. 1605-1612, 2012. [click]

[20] A. M. Zou, K. D. Kumar, Z. G. Hou, and X. Liu, "Finite-time attitude tracking control for spacecraft using terminal sliding mode and Chebyshev neural network," *IEEE Trans. Syst., Man Cybern., Part B: Cybern.,* vol. 41, no. 4, pp. 950-963, 2011. [click]

[21] H. W. Gao, J. G. Liu, Y. M. Li, K. Hong, and Y. Zhang, "Dual-layer fuzzy control architecture for the CAS rover arm," *Int. J. Control, Autom. Syst.*, vol. 13, no. 5, pp. 1-10, 2015.

[22] Y. G. Liu and Y. M. Li, "Dynamic modeling and adaptive neural-fuzzy control for nonholonomic mobile manipulators moving on a slope," *Int. J. Control, Autom. Syst.*, vol. 4, no. 2, pp. 197-203, 2006.

[23] B. F. Francisco, O. Alberto, and O. Gabriel, "Visual navigation for mobile robots: A survey," *J. Intell. & Robot. Syst.*, vol. 53, no. 3, pp. 263-296, 2008. [click]

[24] M. A. Batalin, G. Sukhatme, and M. Hattig, "Mobile robot navigation using a sensor network," *Proc. of IEEE Int. Conf. Robot. Autom.*, pp. 636-641, 2004. [click]

[25] V. Y. Rutkovskii, V. M. Sukhanov, and V. M. Glumov, "Some issues of controlling the free-flying manipulative space robot," *Autom. Remote Control*, vol. 74, no. 11, pp. 1820-1837, 2013. [click]

[26] P. C. Hughes, *Spacecraft Attitude Dynamics*, Dover Publications, 2012.

[27] A. Tayebi and S. McGilvray, "Attitude stabilization of a VTOL quadrotor aircraft," *IEEE Trans. Control Syst. Techn.*, vol. 14, no. 3, pp. 562-571, 2006. [click]

[28] M. G. Zhang and W. H. Li, "Single neuron PID model reference adaptive control based on RBF neural network," *Proc. of 5th IEEE Int. Conf. Mach. Learn. Cybern.*, pp. 3021-3025, 2006.

[29] J. H. Chen and T. C. Huang, "Applying neural networks to on-line updated PID controllers for nonlinear process control," *J. Process Control*, vol. 14, no. 2, pp. 211-230, 2004. [click]

[30] H. L. Shu and Y. G. Pi, "PID neural networks for time-delay systems," *Computers Chem. Eng.*, vol. 24, pp. 859-862, 2000. [click]

[31] H. L. Shu and J. T. Hu, "Study on multivariable system based on PID neural network control," *Adv. Mater. Res.*, vols. 591-593, pp. 1490-1495, 2012. [click]

[32] J. Nandong, "A unified design for feedback-feedforward control system to improve regulatory control performance," *Int. J. Control, Autom., Syst.*, vol. 13, no. 1, pp. 91-98, 2015. [click]

[33] H.-K. Fung, Y.-K. Wong, Y. Ma, C.-W. Yuen, and W.-K. Wong, "Smart hanger dynamic modeling and fuzzy controller design," *Int. J. Control, Autom., Syst.*, vol. 9, no. 4, pp. 691-700, 2011.

[34] Y. Gao and J. G. Liu, "China's robotics successes abound," *Science*, vol. 345, no. 6196, pp. 523, 2014.

[35] Y. R. Tang and Y. M. Li, "Dynamic modeling for high-performance controller design of a UAV quadrotor," *Proc. of IEEE Int. Conf. Inf. Autom.(ICIA)*, Lijiang, Yunnan, China, pp. 3112 - 3117, Aug. 8-10, 2015.

[36] H. Sun, J. G. Liu, Z. Luo, and Y. M. Li, "Dynamic simulation of the vibration isolation system for astronaut treadmill," *Proc. of World Congr. Intell. Control Autom.(WCICA)*, Shenyang, China, pp. 6041-6048, June 29-July 4, 2014.

[37] Y. R. Tang and Y. M. Li, "Design, implementation and control of a small-scale UAV quadrotor," *Proc. of World Congr. Intell. Control Autom.(WCICA)*, Shenyang, China, pp. 2364-2369, June 29-July 4, 2014.

[38] Y. R. Tang and Y. M. Li, "Realization of the flight control for an indoor UAV quadrotor," *Proc. of IEEE Int. Conf. Inform. Autom.(ICIA)*, Yinchuan, Ningxia, China, pp. 1278-1283, August 26-28, 2013.

[39] Y. R. Tang and Y. M. Li, "Design of an optimal flight control system with integral augmented compensator for a nonlinear UAV helicopter," *Proc. of The 10th World Congr. Intell. Control Autom.(WCICA)*, Beijing, China, pp. 3927-3932, July 6-8, 2012.

[40] Y. R. Tang and Y. M. Li, "Development of a laboratory HILs testbed system for small UAV helicopters," *Proc. of The IASTED Int. Conf. Robotics*, Pittsburgh, USA, pp. 428-436, Nov. 7-9, 2011.

[41] Y. R. Tang and Y. M. Li, "The software architecture of a reconfigurable real-time onboard control system for a small UAV helicopter," *Proc. of The 8th Int. Conf. on Ubiq. Robots & Amb. Intell.(URAI)*, Incheon, Korea, pp. 228-233, Nov. 23-26, 2011.

[42] Y. M. Li and Y. G. Liu, "Real-time tip-over prevention and path following control for redundant nonholonomic mobile modular manipulators via fuzzy and neural-fuzzy approaches," *J. Dyn. Syst. Meas. Control*, *ASME Trans.* vol. 128, no. 4, pp. 753-764, Dec., 2006. [click]

[43] X. Chen and Y. M. Li, "Stability on adaptive NN formation control with variant formation patterns and interaction topologies," *Int. J. Adv. Robot. Syst.*, vol. 5, no. 1, pp. 69-82, 2008.

[44] X. Chen and Y. M. Li, "Smooth formation navigation of multiple mobile robots for avoiding moving obstacles," *Int. J. Control, Autom., Syst.*, vol. 4, vo. 4, pp. 466-479, 2006.

[45] Y. G. Liu and Y. M. Li, "Sliding mode adaptive neural-network control for nonholonomic mobile modular manipulators," *J. Intell. & Rob. Syst.,* vol. 44, no. 3, pp. 203-224, Nov. 2005.

Jinguo Liu received his Ph.D. degree in robotics from Shenyang Institute of Automation (SIA), Chinese Academy of Sciences (CAS) in 2007. Since January 2011, he has been a Full Professor with SIA, CAS. He also holds the Assistant Director position of State Key Laboratory of Robotics (China) from March 2008. His research interests include modular robot, rescue robot, space robot, and bio-inspired robot. He has authored and coauthored over eighty papers and thirty patents in above areas.

Qing Gao is a Ph.D. Candidate of Shenyang Institute of Automation (SIA). He received his B.S. degree from Liaoning Technology University. His main research interests include space robot, intelligent control and multi-spacecraft formation flying control.

Zhiwei Liu is a Master student of Shenyang Ligong University and a research assistant in Shenyang Institute of Automation (SIA). His main research interests include robot, the theory and application of the modern mechanical design.

Yangmin Li received his B.S. and M.S. degrees from the Mechanical Engineering Department, Jilin University, Changchun, China, in 1985 and 1988 respectively. He received Ph.D. degree from the Mechanical Engineering Department, Tianjin University, Tianjin, China in 1994. After that, he worked as Postdoctoral Research Associate in Purdue University, USA. He is currently a Full Professor at Faculty of Science and Technology, University of Macau. He is also an Overseas Distinguished Scholar at Shenyang Institute of Automation (SIA), Chinese Academy of Sciences (CAS). His research interests are mobile robots, swarm intelligence, and micro/nano manipulation. Up to now he has published 360 papers in refereed book chapters, journals and conferences. He is an IEEE senior member, a member of ASME and CSME. He is serving as Associate Editor of International Journal of Control, Automation, and Systems, Associate Editor of IEEE Transactions on Automation Science Engineering, Associate Editor of Mechatronics, Council Member and Editor of Chinese Journal of Mechanical Engineering, Associate Editor of IEEE Access. He was a Technical Editor of IEEE/ASME Transactions on Mechatronics.